UNIVERSITÀ DI PARMA

ARCHIVIO DELLA RICERCA

University of Parma Research Repository

Intermolecular Energy Transfer in Real Time

This is the peer reviewd version of the followng article:

Original
Intermolecular Energy Transfer in Real Time / Di Maiolo, Francesco; Painelli, Anna. - In: JOURNAL OF CHEMICAL THEORY AND COMPUTATION. - ISSN 1549-9618. - 14:(2018), pp. 4985-5434. [10.1021/acs.jctc.8b00540]

Availability:
This version is available at: 11381/2849663 since: 2021-10-07T09:03:57Z

Publisher:
American Chemical Society

Published
DOI:10.1021/acs.jctc.8b00540

Terms of use:

Anyone can freely access the full text of works made available as "Open Access". Works made available

Publisher copyright

note finali coverpage

(Article begins on next page)

25 April 2024

This document is confidential and is proprietary to the American Chemical Society and its authors. Do not copy or disclose without written permission. If you have received this item in error, notify the sender and delete all copies.

Intermolecular Energy Transfer in Real Time

Journal:	*Journal of Chemical Theory and Computation*
Manuscript ID	ct-2018-00540y.R1
Manuscript Type:	Article
Date Submitted by the Author:	05-Aug-2018
Complete List of Authors:	Di Maiolo, Francesco; Universita degli Studi di Parma Dipartimento di Chimica, SCVSA Painelli, Anna; Università di Parma, Dip. Chimica GIAF

SCHOLARONE™
Manuscripts

Intermolecular Energy Transfer in Real Time

Francesco Di Maiolo and Anna Painelli*

Department of Chemistry, Life Science and Environmental Sustainability, Università di Parma, 43124 Parma, Italy

E-mail: anna.painelli@unipr.it

Abstract

Resonance energy transfer (RET) is a complex phenomenon where energy is transferred between two non-equivalent molecules. In the Förster picture, that applies to the weak coupling regime, RET occurs from the energy donor molecule in the relaxed excited state towards the acceptor, in an energy-conserving process. However, energy dissipation is crucial for a more general picture of RET that also applies to the strong coupling regime. Here we present a dynamical, non-adiabatic model for RET also accounting for energy relaxation. We exploit the essential state formalism to set up a model for the RET pair that yields an accurate picture of the relevant physics, accounting for just few electronic states and a single coupled vibrational coordinate per molecule. Molecular vibrations are treated in a non-adiabatic approach and energy dissipation is dealt within the Redfield formalism. The approach is first validated on an isolated dye, demonstrating that a very simple relaxation model, defined in terms of a single relaxation parameter, properly describes the different regimes of energy dissipation expected for a molecule, with a fast (fs time window) internal conversion to the lowest excited state and a slow relaxation towards the ground state (ns time window). The same approach is then applied to follow the real time dynamics of a RET pair.

*To whom correspondence should be addressed

In line with the Förster model, in the weak coupling regime the internal conversion of the donor molecule is completed before energy transfer takes place. Our approach also applies to the strong coupling regime, where we observe ultrafast energy transfer occurring well before the internal relaxation of the energy donor is completed.

1 Introduction

Intermolecular energy transfer describes a process where an excited molecule, the energy donor $\mathcal{D}$, transfers its excess energy to a nearby molecule, the energy acceptor $\mathcal{A}$, as follows:[1,2]

$$\mathcal{D}^* + \mathcal{A} \rightarrow \mathcal{D} + \mathcal{A}^*, \tag{1}$$

where the star marks excited species. When the energy donor and acceptor species are located at larger distances than the wavelength of light, energy transfer occurs via a trivial radiative process, mediated by the exchange of a photon. At shorter distances, radiationless energy transfer takes place, a more interesting phenomenon, governed by two mechanisms: the Dexter mechanism that, involving the coordinated transfer of electrons between the two molecules, applies for intermolecular distances shorter than 3-4 Å and the Resonance Energy Transfer (RET) mechanism that, implying the exchange of a virtual photon, occurs for intermolecular distances up to ∼100 Å and is driven by electrostatic interactions. RET plays a prominent role in technological applications[3–9] and governs several biological processes.[10–14] The mechanism of the fast and efficient RET in photosynthetic centers is presently not fully understood, in spite of the enormous amount of experimental and theoretical work.[15–17]

The first theoretical approach to RET dates back to the work of Förster in 1948[18–21] and is crucially based on several approximations. Electrostatic interactions are modeled by Förster in the dipolar approximation and are treated perturbatively, a clever choice that allowed him to directly relate RET probability to experimentally accessible quantities (i.e., the oscillator strength). However the two approximations are bound to fail for short intermolec-

ular distances, as discussed in several recent papers.[22–30] Moreover Förster model assumes that RET takes place only after all slow degrees of freedom, including molecular vibrations and polar solvation, are fully relaxed to their equilibrium positions as relevant to the excited $\mathcal{D}^*$ species. In other terms, RET, as modeled by Förster, describes an incoherent process occurring from the relaxed excited state of $\mathcal{D}$ towards $\mathcal{A}$. Accordingly, Förster theory of RET is static in nature. To develop dynamical models of RET, the concurrent dynamics of several degrees of freedom must be described, also accounting for relaxation, i.e. for dissipative phenomena. A true dynamical model for RET then requires entering the realm of open quantum systems, i.e. quantum systems, $\mathcal{S}$, interacting and exchanging energy with the environment (called the bath, $\mathcal{B}$).[31,32] The first problem to be faced in this context is the proper definition of the system vs the bath. Dynamical theories of RET often collapse all degrees of freedom, including high energy degrees of freedom, molecular vibrations, conformational and solvent coordinates into the bath.[33,34] This approach however smears out many details and does not allow to appreciate the different role of fast environmental fluctuations (typically in the ultraviolet spectral region), of molecular vibrations (typically in the mid-infrared region) and of much slower motions related to conformational and polar solvation degrees of freedom.[7,35] Moreover, in the strong coupling regime, the timescales of vibrational relaxation and of RET dynamics become comparable, making the Markov approximation untenable.[36] Recently, a modified Redfield approach was proposed to overcome this problem.[37]

In this work we discuss dynamic RET in a model system where molecular vibrations are explicitly accounted in a non-adiabatic approach so that RET can be described in the same theoretical framework for both the weak and strong coupling regimes. We adopt the Redfield formalism to describe relaxation dynamics. Accordingly, we consider a bath weakly coupled to the system and assume that the dynamics of the bath degrees of freedom is much faster than relevant processes (Marcov regime).[31] In other terms, we describe homogeneous broadening effects or intrinsic lifetimes, due to the coupling between the degrees of freedom explicitly accounted for in the model (low-lying electronic excitations and molecular

vibrations) and the fast environmental degrees of freedom (in our case the electronic degrees of freedom of the solvent and the high-energy molecular excitations). The effects of slow variables as relevant to inhomogeneous broadening, including polar solvation and molecular conformational modes, cannot be discussed within this framework and will be addressd in a separate publication.

In Section 2, we introduce a simple, yet realistic model for the RET pair where both the energy donor and acceptor molecules are described in the essential state model (ESM) formalism in terms of just two electronic states coupled to a single vibrational coordinate. ESMs offer a reliable description of optical spectra of organic dyes in different environments and quantitatively account for polar solvation.[38–42] Moreover, ESMs offer a quantitative and non-perturbative description of electrostatic intermolecular interactions in molecular aggregates[43–45] and RET systems.[30,46] In Section 3, we will validate our approach to dissipative dynamics working on a single molecule. Section 4 summarizes the central results of this paper, illustrating the RET dynamics on a $\mathcal{DA}$ pair. Crucially, Section 4.2 will address ultrafast RET beyond the Förster regime. A discussion and conclusion Section will shortly summarize the main results, setting the stage for future developments.

2 The models

2.1 The molecular model

Electron donor-acceptor or push-pull chromophores are π-conjugated molecules decorated with an electron-donor (D) and an electron-acceptor (A) group (not to be confused with energy donor, $\mathcal{D}$, and energy acceptor, $\mathcal{A}$), to give polar (D-π-A) structures. 4-Dimethylamino-4'-nitrostilbene (DANS) and 9-diethylamino-5-benzo[α]phenoxazinone (Nile Red) in Fig.1c and d are typical examples. Low-energy spectra of push-pull dyes are successfully described in terms of just two diabatic electronic states, $|N\rangle$ and $|Z\rangle$, corresponding to the neutral D-π-A and to the zwitterionic D^+-π-A^- forms, respectively.[39,47] The two states, separated

by an energy gap $2z$, are mixed by the matrix element $-\tau$ to give a ground and an excited states (see Fig.1a):

$$\begin{aligned} |G\rangle &= \sqrt{1-\rho}|N\rangle + \sqrt{\rho}|Z\rangle, \\ |E\rangle &= \sqrt{\rho}|N\rangle - \sqrt{1-\rho}|Z\rangle, \end{aligned} \tag{2}$$

where $\rho = 0.5(1 - z/\sqrt{z^2+\tau^2})$ is the ground state expectation value of the ionicity operator $\hat{\rho}$=$|Z\rangle\langle Z|$, measuring the polarity of the dye. The states $|G\rangle$ and $|E\rangle$ in the above equations are the adiabatic states, relevant to spectroscopy and to RET, and correspond to the $|\mathcal{D}\rangle$ and $|\mathcal{D}^*\rangle$ states of the energy-donor molecule or to the $|\mathcal{A}\rangle$ and $|\mathcal{A}^*\rangle$ states of the energy-acceptor. The dipole moment operator is easily defined on the diabatic basis. Indeed, the permament dipole moment associated with the $|Z\rangle$ state, μ_0, is much larger than all other matrix elements of the dipole moment operator, that are therefore neglected, setting $\hat{\mu}$=$\mu_0\hat{\rho}$.[48] With this approximation, the transition energy and the transition dipole moment read $\hbar\omega_{CT} = \tau/\sqrt{\rho(1-\rho)}$ and $\mu_{CT} = \mu_0\sqrt{\rho(1-\rho)}$.[39,47]

Within ESMs, the coupling between electronic and vibrational degrees of freedom is introduced in D-π-A dyes accounting for a single effective vibration linearly coupled to the electronic states.[39,47] Accordingly, two harmonic potential energy curves are assigned to the two diabatic states, with the same frequency ω_v, but displaced minima (linear electron-vibration coupling). The molecular Hamiltonian thus reads:

$$\hat{H} = -\tau\hat{\sigma} + \left[2z - \sqrt{\hbar\omega_v\varepsilon_v}(\hat{d}^\dagger + \hat{d})\right]\hat{\rho} + \hbar\omega_v\left(\hat{d}^\dagger\hat{d} + \frac{1}{2}\right), \tag{3}$$

where $\hat{\sigma} = |N\rangle\langle Z| + |Z\rangle\langle N|$ is the hopping operator, $\hat{d}^\dagger$ and $\hat{d}$ are the creation and annihilation operators of the harmonic oscillator and ε_v is the vibrational relaxation energy. In the following we define the dimensionless vibrational coordinate as $\hat{Q} = \hat{d}^\dagger + \hat{d}$.[49,50] The dimensional coordinate as usually defined in spectroscopy is $\hat{Q}_S = \sqrt{\hbar/2\omega_v}\hat{Q}$.

Accounting for a single coupled coordinate may appear a dramatic approximation, yet

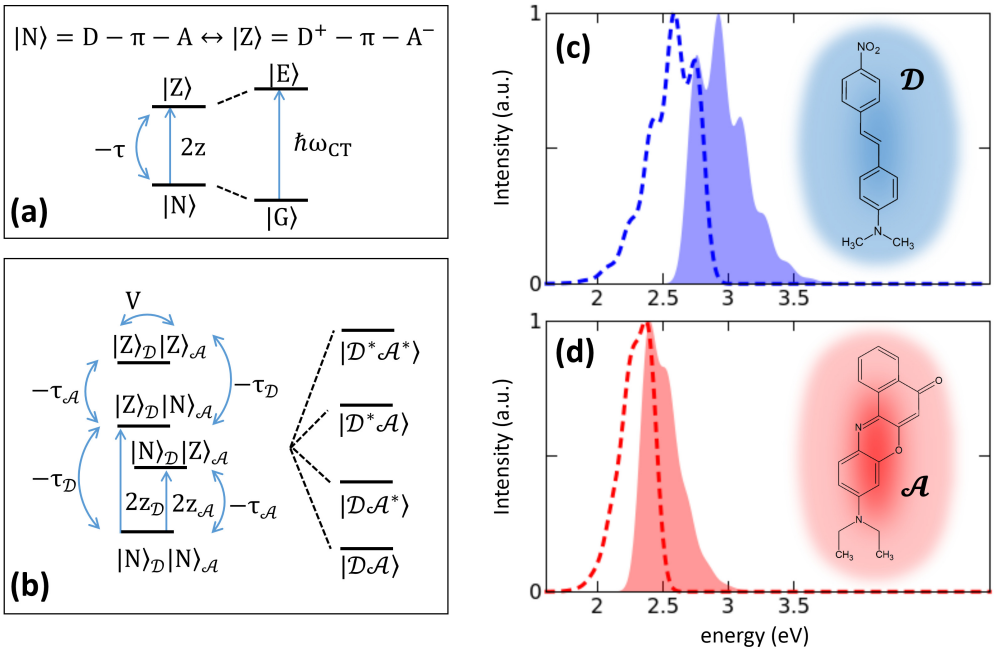

Figure 1: Essential state models. (a) Sketch of the two-states electronic model for an isolated dye; (b) sketch of the four-states electronic model used to describe two interacting dyes; (c) calculated optical absorption (color filled area) and emission (dashed curve) spectra of DANS in a non-polar solvent; (d) the same as (c) for Nile Red. A Gaussian bandshape with half width at half maximum (HWHM) equal to 0.076 eV is assigned to each vibronic transition in the calculation of spectra in (c) and (d). Other molecular parameters are reported in Tab.1.

the Hamiltonian in Eq.3 accurately describes experimental spectra of several dyes, accounting for the vibronic bandshapes observed in linear and non-linear optical spectra of D-π-A dyes in good detail.[39,40,45,47] From a theoretical perspective, rigorous methods to decimate the number of coupled coordinates in complex molecular systems have been discussed and successfully implemented by several authors in recent years.[51–54]

Adiabatic solutions of the above Hamiltonian are available and in this approximation analytical results may be obtained. However, since the two potential energy curves associated with the ground and excited electronic states are markedly anharmonic,[47,55] the calculation of vibrational eigenstates becomes cumbersome and a non-adiabatic approach, based on the brute force diagonalization, is more expedited. On the other hand, a non-adiabatic approach is the only viable solution to calculate optical spectra of molecular aggregates or of RET systems.[45,56]

In the non-adiabatic approach, we write Eq.3 on the vector space defined as the direct product of the two-dimensional electronic Hilbert space times the ∞-dimensional Fock space spanned by the eigenstates of the harmonic oscillator. In order to make the problem numerically tractable, we truncate the Fock space to the m lowest vibrational excitations, with m large enough as to reach convergence on the properties of interest (typically, we will show results for m $\sim$15-16). The eigenstates of the Hamiltonian matrix are the non-adiabatic vibronic eigenstates, $|\phi_k\rangle$, that enter the calculation of spectral properties. Steady-state absorption spectra can be calculated based on transition energies and relevant squared transition dipole moments $|\langle\phi_1|\hat{\mu}|\phi_k\rangle|^2$, for k=$2, ..., 2m$, where $\hat{\mu}$ is the dipole moment operator projected on the non-adiabatic basis. Non-linear optical spectra can also be easily addressed via the calculation of the complete matrix representing the dipole moment operator on the molecular eigenstates.[45] The non-adiabatic fluorescence spectrum requires the transition dipole moments from the fluorescent state $|\langle\phi_f|\hat{\mu}|\phi_k\rangle|^2$, for k=$1, ..., f-1$. Since the electronic transitions are much more intense than vibrational transitions, we single out the fluorescent state, $|\phi_f\rangle$, as the lowest excited state with a sizable transition dipole moment from the ground state.[57] Alternatively, a calculation of the dissipative dynamics of the dye, following optical excitation (see below), allows to single out the fluorescent state as the quasi-stationary state. Fig.1c, d shows absorption and fluorescence spectra calculated for DANS and Nile Red. Relevant model parameters (Table 1) are taken from the literature, and were obtained via a careful fit of linear and non-linear spectra of the two dyes in different solvents.[38,45,57]

Table 1: Model parameters for DANS[45] and Nile Red.[38] All the quantities are in eV.

	$2z$	τ	ε_v	$\hbar\omega_v$
DANS	2.64	0.72	0.3	0.17
Nile Red	1.76	0.95	0.33	0.14

2.2 The RET model

We consider a RET pair constituted by two different D-π-A dyes, playing the role of energy donor, $\mathcal{D}$, and of energy acceptor, $\mathcal{A}$. The diabatic basis for the RET pair is the direct product of the basis states of the isolated dyes. We therefore end up with 4 electronic states: $|N_{\mathcal{D}}N_{\mathcal{A}}\rangle$, $|Z_{\mathcal{D}}N_{\mathcal{A}}\rangle$, $|N_{\mathcal{D}}Z_{\mathcal{A}}\rangle$, $|Z_{\mathcal{D}}Z_{\mathcal{A}}\rangle$, as sketched in Fig.1b. To describe RET we only account for electrostatic intermolecular interactions, that, in line with the negligible polarity of the molecular $|N\rangle$ states, are fully described by a single parameter V that measures the interaction between the two molecules when both are in the zwitterionic state. Accordingly, the electronic Hamiltonian for the RET pair reads:

$$\hat{H}_{el}^{\mathcal{DA}} = -\tau_{\mathcal{D}}\hat{\sigma}_{\mathcal{D}} + 2z_{\mathcal{D}}\hat{\rho}_{\mathcal{D}} - \tau_{\mathcal{A}}\hat{\sigma}_{\mathcal{A}} + 2z_{\mathcal{A}}\hat{\rho}_{\mathcal{A}} + V\hat{\rho}_{\mathcal{D}}\hat{\rho}_{\mathcal{A}}, \quad (4)$$

where $\hat{\sigma}_{\mathcal{D}(\mathcal{A})}$ and $\hat{\rho}_{\mathcal{D}(\mathcal{A})}$ are the energy donor (energy acceptor) hopping and ionicity operators, respectively, $2z_{\mathcal{D}(\mathcal{A})}$ is the energy associated with the energy donor (energy acceptor) zwitterionic state, while $\tau_{\mathcal{D}(\mathcal{A})}$ is the relevant CT integral. The first four terms in the above Hamiltonian are the sum of the two electronic molecular Hamiltonians, and the last term describes electrostatic intermolecular interactions. Numerical diagonalization of $\hat{H}_{el}^{\mathcal{DA}}$ leads to four electronic eigenstates that, for not too large V values are readily identified as $|\mathcal{DA}\rangle$, $|\mathcal{DA}^*\rangle$, $|\mathcal{D}^*\mathcal{A}\rangle$, $|\mathcal{D}^*\mathcal{A}^*\rangle$, where the star is used for the excited species.

The RET Hamiltonian in Eq.4 describes two dyes interacting via electrostatic intermolecular interactions, so that it must describe the same physics as standard RET models. This can be made explicit rewriting the Hamiltonian in Eq.4 in the *exciton basis*,[43] i.e. the basis defined for each dye, by the $|G\rangle$ and $|E\rangle$ electronic eigenstates in Eq.2. On this basis, we can calculate the interaction between the two states involved in RET as $\langle G_{\mathcal{D}}E_{\mathcal{A}}|V\hat{\rho}_{\mathcal{D}}\hat{\rho}_{\mathcal{A}}|E_{\mathcal{D}}G_{\mathcal{A}}\rangle = V\sqrt{\rho_{\mathcal{D}}(1-\rho_{\mathcal{D}})}\sqrt{\rho_{\mathcal{A}}(1-\rho_{\mathcal{A}})}$. If V, the electrostatic interaction energy between the two molecules in the zwitterionic state, is written in the dipolar approximation, the RET matrix elements just describe the interaction between the two transition

dipole moments, as in the standard Förster form model.[30,46]

To complete the model, in line with the approach described above for the isolated dye, we introduce an effective molecular vibration for both $\mathcal{D}$ and $\mathcal{A}$, with coordinates $\hat{Q}_{\mathcal{D}}$ and $\hat{Q}_{\mathcal{A}}$, respectively. The complete Hamiltonian for the RET pair then reads:

$$\hat{H}_{\mathcal{DA}} = \hat{H}_{el}^{\mathcal{DA}} - g_{\mathcal{D}}\hat{\rho}_{\mathcal{D}}(\hat{d}^{\dagger}+\hat{d}) - g_{\mathcal{A}}\hat{\rho}_{\mathcal{A}}(\hat{a}^{\dagger}+\hat{a}) + \hbar\omega_v^{\mathcal{D}}\left(\hat{d}^{\dagger}\hat{d}+\frac{1}{2}\right) + \hbar\omega_v^{\mathcal{A}}\left(\hat{a}^{\dagger}\hat{a}+\frac{1}{2}\right), \quad (5)$$

where $\hat{d}^{\dagger}$ and $\hat{a}^{\dagger}$ are the boson creation operators relevant to the harmonic oscillator on $\mathcal{D}$ and $\mathcal{A}$, respectively, $\omega_v^{\mathcal{D}(\mathcal{A})}$ is the vibrational frequency of the $\mathcal{D}$ ($\mathcal{A}$) molecule and $g_{\mathcal{D}(\mathcal{A})}=\sqrt{\hbar\omega_v^{\mathcal{D}(\mathcal{A})}\varepsilon_{\mathcal{D}(\mathcal{A})}}$ is the $\mathcal{D}(\mathcal{A})$ electron-vibrational coupling strength, $\varepsilon_{\mathcal{D}(\mathcal{A})}$ being the relevant vibrational relaxation energy.

Adopting the same strategy discussed in Sect.2.1 for the isolated molecule, Eq.5 is written on the vector space defined as the direct product of the 4-fold electronic Hilbert space times the two Fock spaces associated with the molecular coordinates $\hat{Q}_{\mathcal{D}}$ and $\hat{Q}_{\mathcal{A}}$. We present results obtained truncating the Fock spaces in such a way that the sum of vibrational quanta on the $\mathcal{D}$ and $\mathcal{A}$ oscillators does not exceed 16. The resulting Hamiltonian is a 544×544 sparse matrix.

In the following, we will describe RET in the $\mathcal{DA}$ pair formed by DANS (the energy donor) and Nile Red (the energy acceptor), adopting molecular model parameters in Table 1. Different values of the $\mathcal{DA}$ interaction will be considered, ranging from the weak coupling regime (V=0.08 eV), where RET occurs from the relaxed $\mathcal{D}^*$ state, in line with the Förster model, to the strong coupling limit (V=0.3 and 0.6 eV) where RET occurs from a hot $\mathcal{D}^*$ state.

3 Dissipative quantum dynamics for a single molecule

We start studying energy dissipation and relaxation phenomena in an isolated dye, representing either the energy donor or the energy acceptor. In the following, we will present specific

results for DANS, that will later represent the energy donor in the RET pair. Similar results can be obtained for other dyes. Results for Nile Red, that in the following will be used as the energy acceptor, are collected in the Supporting Information (SI).

The molecular Hamiltonian for the dye is described in Eq.3 and we prepare the out of equilibrium state by impulsive excitation. In the hypothesis that only the molecular ground state is populated at the equilibrium, we write the coherent excited state at time zero as:[58]

$$|\Psi^*(t=0)\rangle \quad \propto \quad \sum_{k=2}^{N} |\phi_k\rangle\langle\phi_k|\hat{\mu}|\phi_1\rangle, \tag{6}$$

where the sum runs over all the excited non-adiabatic eigenstates of the system of interest, $\mathcal{S}$. If the $\mathcal{SB}$ interaction term, $\hat{H}_I$, is switched off, the time evolution of the excited state is trivially determined by the Hamiltonian in Eq.3 and the system energy is conserved.[58] When the coupling with the environment is switched on, the dye starts exchanging energy with the surrounding and specific approaches must be adopted to deal with open quantum systems.

Here we are interested to discuss dissipation as due to the interaction of relevant molecular degrees of freedom (low-lying electronic excitations and molecular vibrations) as described in our ESM model with fast degrees of freedom, namely high energy electronic fluctuations in either the dye itself or in the surrounding solvent. This fast motion is responsible for quick fluctuations of the energies of the system eigenstates, so that an energy exchange sets in, but in a so fast scale of time as to be factorized. In spectroscopic language, fast degrees of freedom are responsible for homogeneous broadening, and hence for the finite lifetime of excited states. The Redfield approach offers a strategy to decribe homogeneous broadening, modeling the effects of the fluctuating environment in terms of a bath of quantum harmonic oscillators:

$$\hat{H}_{\mathcal{B}} \quad = \quad \sum_i \hbar\omega_i \Big(\hat{b}_i^\dagger \hat{b}_i + \frac{1}{2}\Big), \tag{7}$$

where $\hat{b}_i^\dagger$ and $\hat{b}_i$ are the creation and annihilation bosonic operators associated with the i-th bath oscillator, with frequency ω_i. The bath can exchange energy quanta back and forth with the system as described by the following $\mathcal{SB}$ interaction Hamiltonian, bilinear in the boson operators:[59,60]

$$\hat{H}_I = \sum_i (g_i \hat{b}_i^\dagger \hat{d} + g_i^* \hat{b}_i \hat{d}^\dagger), \tag{8}$$

where g_i is the coupling constant relevant to the i-th bath mode and $\hat{d}^\dagger$ and $\hat{d}$ are the creation and annihilation bosonic operators associated with the molecular oscillator.

At time zero the system is prepared in the coherent state $|\Psi^*\rangle$ defined in Eq.6, corresponding to the reduced density matrix $\hat{\sigma}(0) = |\Psi^*\rangle\langle\Psi^*|$. The subsequent system dynamics is described by the Redfield equation:[61]

$$\frac{d}{dt}\sigma_{ab}(t) = -i\omega_{ab}\sigma_{ab}(t) + \sum_{c,d} R_{ab,cd}\sigma_{cd}(t), \quad \forall a,b = 1,...,N, \tag{9}$$

where $\sigma_{ab}(t) = \langle\phi_a|\hat{\sigma}(t)|\phi_b\rangle$ is the matrix element of the reduced density matrix written on the eigenstates of the system Hamiltonian in Eq.3, and $\omega_{ab} = (E_a - E_b)/\hbar$ is the relevant transition frequency. The Redfield relaxation super-operator has elements:

$$R_{ab,cd} = -\delta_{b,d}\sum_e \Gamma^+_{ae,ec} - \delta_{a,c}\sum_e \Gamma^-_{de,eb} + \Gamma^+_{db,ac} + \Gamma^-_{db,ac}, \tag{10}$$

where $\delta_{b,d}$ and $\delta_{a,c}$ are Kronecker delta symbols.

The Redfield dissipative dynamics is therefore governed by the kinetic coefficient tensors, $\mathbf{\Gamma}^+$ and $\mathbf{\Gamma}^-$. To estimate the relaxation tensors, we introduce the Bose-Einstein distribution for the bath phonons, $\langle\hat{n}(\omega_{ac})\rangle_b = (exp[\beta\hbar\omega_{ac}] - 1)^{-1}$ and an explicit expression for the bath spectral density $\mathcal{J}(\omega) = \sum_i |g_i|^2\delta(\omega - \omega_i)$. Since we are interested to model fast environmental degrees of freedom, we assume a constant bath spectral density (or at least we assume that the phonon distribution falls off with ω much faster than the bath spectral

density), so that $\mathcal{J}(\omega) = \hbar^2\gamma/\pi$.[60,62] Accordingly, the kinetic coefficients read:

$$\Gamma^{+}_{db,ac} = \gamma\Big(d_{db}d^{\dagger}_{ac}\langle\hat{n}(\omega_{ac})\rangle_b + d^{\dagger}_{db}d_{ac}\langle\hat{n}(\omega_{ca})+1\rangle_b\Big), \quad (11)$$

$$\Gamma^{-}_{db,ac} = \gamma\Big(d_{db}d^{\dagger}_{ac}\langle\hat{n}(\omega_{bd})\rangle_b + d^{\dagger}_{db}d_{ac}\langle\hat{n}(\omega_{db})+1\rangle_b\Big), \quad (12)$$

where $d^{(\dagger)}_{ac} = \langle\phi_a|\hat{d}^{(\dagger)}|\phi_c\rangle$ is the matrix element of $\hat{d}^{(\dagger)}$ written on system eigenstates. The coefficients $\Gamma^{+}_{db,ac}$ and $\Gamma^{-}_{db,ac}$ describe the exchange of vibrational quanta between $\mathcal{S}$ and $\mathcal{B}$. Specifically, terms containing $\langle\hat{n}(\omega_{ca}+1)\rangle_b$, describe one vibrational quantum emitted by the system, while terms containing $\langle\hat{n}(\omega_{ac})\rangle_b$ describe the absorption of one reservoir phonon by the system. With this choice of the bath spectral density, the dissipative dynamics is defined by a single phenomenological paramer, γ.

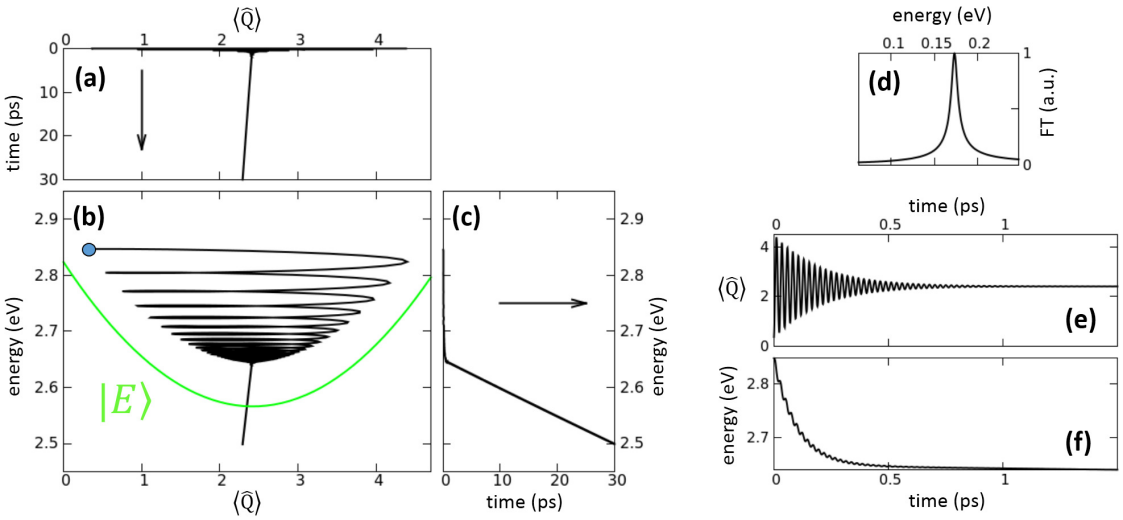

Figure 2: Isolated dye: decoherence and energy dissipation following coherent excitation. (a) Time-evolution of the expectation value of the molecular coordinate; (b) evolution of the system energy as a function of the expectation value of the molecular coordinate; the blue point marks the starting point of the dynamics. The green curve is the adiabatic excited state potential energy curve and is shown for reference; (c) time-dependence of the system energy; (d) Fourier transform of the signal in panel e; (e and f) early-stage dynamics of the molecular coordinate and system energy, respectively. Calculations are done for the molecular parameters reported in the first row of Table 1, as relevant to DANS molecule, and accounting for 16 vibrational states. All other parameters are defined in the main text.

In Fig.2, we show results obtained solving the Redfield equation using the Short-Iterative-

Arnoldi algorithm[63,64] (Δt=1 fs as time step) for a coherently excited dye described by the molecular parameters in the first row of Table 1 interacting with a bath at 298 K and setting γ= 5 ps^{-1}. The calculated dissipative dynamics is very clearly divided into two main phases. In the first phase a very fast energy dissipation towards the lowest excited state is observed, that can be fitted with an exponential decay with characteristic time $\sim$ 100 fs. In this regime vibrational quanta are exchanged with the bath, until the system reaches the first vibrational state of the electronic excited state (panels b, c and f). After that, a much slower dynamics sets in, that can be fitted with an exponential decay with characteristic time $\sim$ 0.5 ns, and that describes the decay towards the ground state. Recognizing the two regimes of fast internal conversion to the lowest excited state and of slow relaxation towards the ground state is a highly non-trivial result particularly in view of the very simple model adopted for the relaxation dynamics where the coupling between the system and the Redfield bath is described in terms of a single phenomenological parameter, γ.

Coherent oscillations are observed in the early dynamics, as clearly shown in Fig.2e. The Fourier transform of $\langle \hat{Q}(t) \rangle$ has a peak at 0.174 eV (Fig.2d), corresponding to a slightly higher frequency than the bare vibrational frequency, ω_v (see Table 1), as due to the well-known vibrational hardening of the electronic excited state.[38–42] As time proceeds, $\mathcal{SB}$ correlations develop and after $\sim$500 fs the coherent motion is washed out and the system enters an incoherent regime (panels a, b and e).

The Redfield approach is elegant and powerful, but it is computationally demanding especially for the large basis needed for non-adiabatic dynamics. It is therefore important to devise approximation strategies to make the calculation of Redfield dynamics faster.[65] In the secular approximation, rapidly oscillating $R_{ab,cd}$ components are neglected so that only $R_{aa,cc}$ and $R_{ab,ab}$ terms survive together with those few special $R_{ab,cd}$ elements that satisfy the resonance condition $|\omega_{ab} - \omega_{cd}| = 0$. If only $R_{aa,cc}$ and $R_{ab,ab}$ components are kept, the Redfield equation boils down to the Bloch model, with fully decoupled populations and coherences.[66,67]

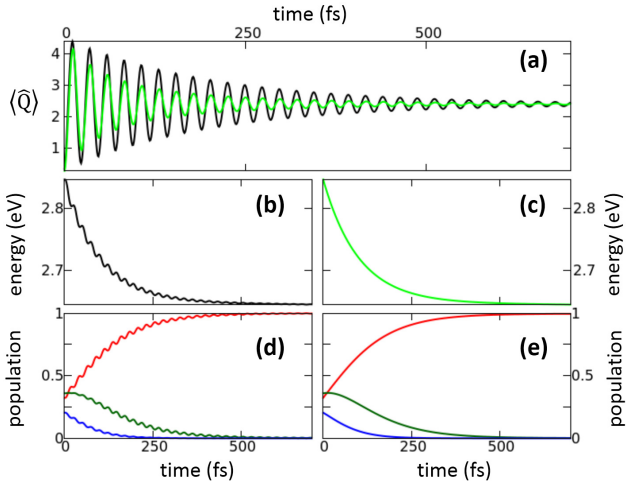

Figure 3: Signatures of population-coherence coupling. (a) Time-dependence of the average value of the molecular coordinate calculated in the Redfield approach (black curve) and in the Bloch approximation (green curve). (b and c) Time-evolution of the system energy using Redfield and the Bloch models, respectively. (d and e) $\sigma_{17,17}(t)$ (red curve), $\sigma_{18,18}(t)$ (dark-green curve), $\sigma_{19,19}(t)$ (blue curve), as relevant to the initially most populated states, using Redfield and the Bloch models, respectively. Same parameters as in Fig.2.

In Fig.3, we compare the dynamics calculated using the complete Redfield equation and adopting the Bloch approximation for the same system studied in Fig.2. The faster decay of the excited state coherence observed in Fig.3a for the Bloch model with respect to the Redfield approach is hardly surprising; indeed, in Redfield equation coherences can be reinforced by processes that turn populations into coherences ($R_{aa,cd}$) as well as by coherence transfer processes ($R_{ab,cd}$). Similarly, in the complete Redfield approach oscillations are observed in the early time dynamics of the energy and of the populations (Fig.3b,d). These oscillations are a clear signature of the population-coherence coupling and are completely lost in the Bloch model (Fig.3c,e). Once the coherences are relaxed, the effect of population-coherence coupling becomes negligible and the long-term dynamics calculated in the Bloch model becomes indistinguishable from the one calculated in the complete Redfield approach.

Before closing this Section, we underline that the proposed model for the relaxation dynamics of the isolated molecule is very similar to the model for relaxation in a vibronic system as discussed by Roden et al. in Ref.[60] However, Roden considers two electronic

states described in the adiabatic approximation by two harmonic potential energy curves with displaced minima. Accordingly, they can only address the vibrational relaxation within each potential energy curve (corresponding to the fast initial relaxation in our system), but cannot model the relaxation from the excited towards the ground states (the slower process in our model). Moreover, in order to properly describe the relaxation on the excited state, they must introduce an ad hoc coupling between the system and the bath, so that the bath is coupled to the undisplaced or to the displaced vibrational coordinate when dealing with the ground or the excited state, respectively. In our ESM for the isolated molecule we introduce two harmonic and displaced potential energy surfaces to describe the diabatic states and we calculate the truly non-adiabatic dynamics of the coupled electron-vibration system. Having a more detailed molecular model, the coupling between the vibrational coordinate and the bath modes needs not to explicitly account for the displacement of the vibrational coordinate when going from the ground to the excited states (see Eq.8), the non-adiabatic solution of the coupled electron-vibration system fully accounting for the displacements.

4 RET: a non-adiabatic dynamical description

We are now ready to discuss our dynamical and non-adiabatic approach to RET. The system Hamiltonian in Eq.5 describes the $\mathcal{DA}$ pair, where the energy donor and acceptor molecules correspond to DANS and Nile Red dyes, respectively, parametrized as discussed above. Along the same lines described for an isolated molecule in Sect.3, a bath of quantum harmonic oscillators is coupled to the RET pair, the interaction Hamiltonian being:

$$\hat{H}_I = \sum_i \left[g_i \hat{b}_i^\dagger (\hat{d} + \hat{a}) + g_i^* \hat{b}_i (\hat{d}^\dagger + \hat{a}^\dagger) \right], \tag{13}$$

where g_i is the interaction strength between the i-th bath coordinate and the $\mathcal{D}$ or $\mathcal{A}$ coordinate (we assume the same coupling for both coordinates). Explicit expressions for the

kinetic coefficients read:

$$\begin{aligned}\Gamma^{+}_{db,ac} &= \gamma\Big[d_{db}d^{\dagger}_{ac}\langle\hat{n}(\omega_{ac})\rangle_b + d^{\dagger}_{db}d_{ac}\langle\hat{n}(\omega_{ca})+1\rangle_b \\ &+ a_{db}a^{\dagger}_{ac}\langle\hat{n}(\omega_{ac})\rangle_b + a^{\dagger}_{db}a_{ac}\langle\hat{n}(\omega_{ca})+1\rangle_b \\ &+ d_{db}a^{\dagger}_{ac}\langle\hat{n}(\omega_{ac})\rangle_b + d^{\dagger}_{db}a_{ac}\langle\hat{n}(\omega_{ca})+1\rangle_b \\ &+ a_{db}d^{\dagger}_{ac}\langle\hat{n}(\omega_{ac})\rangle_b + a^{\dagger}_{db}d_{ac}\langle\hat{n}(\omega_{ca})+1\rangle_b\Big], \qquad (14)\end{aligned}$$

and

$$\begin{aligned}\Gamma^{-}_{db,ac} &= \gamma\Big[d_{db}d^{\dagger}_{ac}\langle\hat{n}(\omega_{bd})\rangle_b + d^{\dagger}_{db}d_{ac}\langle\hat{n}(\omega_{db})+1\rangle_b \\ &+ a_{db}a^{\dagger}_{ac}\langle\hat{n}(\omega_{bd})\rangle_b + a^{\dagger}_{db}a_{ac}\langle\hat{n}(\omega_{db})+1\rangle_b \\ &+ d_{db}a^{\dagger}_{ac}\langle\hat{n}(\omega_{bd})\rangle_b + d^{\dagger}_{db}a_{ac}\langle\hat{n}(\omega_{db})+1\rangle_b \\ &+ a_{db}d^{\dagger}_{ac}\langle\hat{n}(\omega_{bd})\rangle_b + a^{\dagger}_{db}d_{ac}\langle\hat{n}(\omega_{db})+1\rangle_b\Big], \qquad (15)\end{aligned}$$

where $d^{(\dagger)}_{ac} = \langle\phi_a|\hat{d}^{(\dagger)}|\phi_c\rangle$ and $a^{(\dagger)}_{db} = \langle\phi_d|\hat{a}^{(\dagger)}|\phi_b\rangle$ are the matrix elements of $\mathcal{D}$ and $\mathcal{A}$ annihilation (creation) operators, respectively, written on $\hat{H}_{\mathcal{DA}}$ non-adiabatic eigenstates.

Redfield dissipative dynamics can be calculated for the RET pair plugging Eqs.14 and 15 into Eq.10 and solving the dynamics of the reduced density matrix. In all calculations the dynamics starts from a coherent state created upon impulsive excitation according to Eq.6, where $\hat{\mu}$ refers to the dipole moment operator relevant to the $\mathcal{D}$ species, as to ensure an excitation localized on the energy donor species. Results are marginally dependent on the specific choice of the excitation process (see SI).

4.1 Weak coupling regime

We start our analysis discussing the weak coupling regime. In Fig.4, we show results obtained for V=0.08 eV and γ=5 ps^{-1}. The integration step was fixed to Δt=1.5 fs. Since we start from an excitation localized on the energy donor, we initially observe coherent oscillations

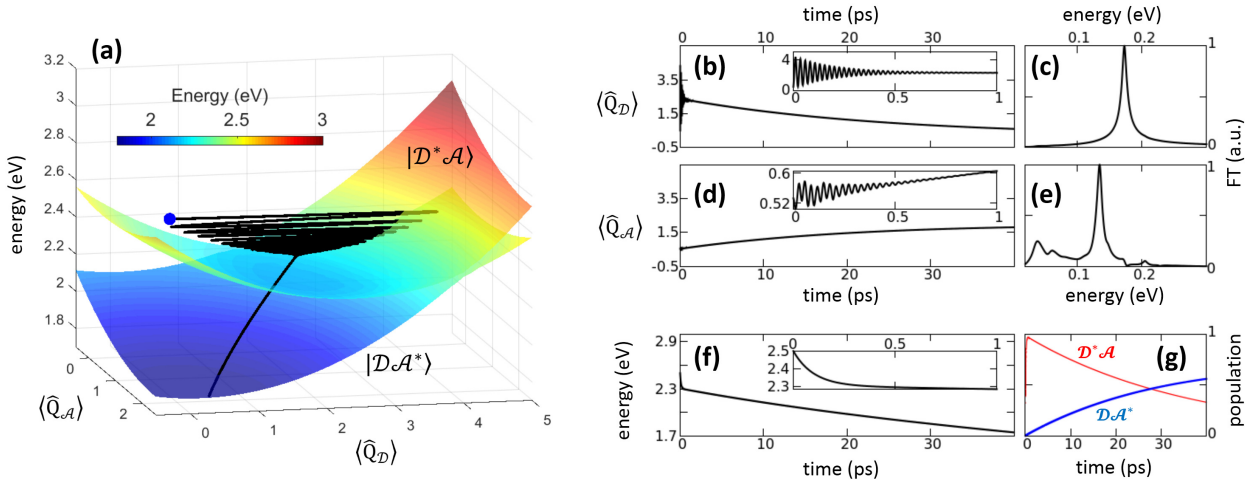

Figure 4: RET dynamics calculated for molecular parameters shown in Tab.1 and V=0.08 eV. (a) Evolution of the energy of the RET pair plotted as a function of the molecular coordinates; the blue dot marks the starting point of the evolution. Adiabatic potential energy surfaces relevant to $|\mathcal{D}^*\mathcal{A}\rangle$ and $|\mathcal{D}\mathcal{A}^*\rangle$ are shown for reference; (b and d) temporal evolution of the expectation values of the $\mathcal{D}$ and $\mathcal{A}$ coordinates, respectively. Relevant insets show the early-stage dynamics; (c and e) Fourier transforms of the signals in panels b and d, respectively; (f) energy of the RET pair as a function of time, with its early-stage dynamics shown in the inset; (g) time evolution of the populations of the two states most involved in the RET process. The maximum number of vibrational excitations is set to 16. Other parameters are defined in the main text.

of $\hat{Q}_\mathcal{D}$ (Fig.4a,b). The relevant Fourier transform peaks at 0.173 eV (Fig.4c), corresponding to oscillations on the $|\mathcal{D}^*\mathcal{A}\rangle$ potential energy surface. In the same early time window, the acceptor coordinate, $\hat{Q}_\mathcal{A}$, shows very weak displacements (inset in Fig.4d). The interaction with the environment destroys the coherence in the first 500 fs (inset in Fig.4b), while the system relaxes to the lowest vibrational state of the donor electronic excited state (Fig.4a,f). After ∼1 ps, the energy starts to slowly flow towards the energy acceptor, as demonstrated by the overall displacement of the $\hat{Q}_\mathcal{A}$ coordinate (Fig.4d). The corresponding Fourier transform (Fig.4e) peaks at ∼0.14 eV, in line with the expected energy of vibrational oscillations on the $|\mathcal{D}\mathcal{A}^*\rangle$ potential energy surface. The energy transfer is better located looking at the time evolution of the populations in Fig.4g. Initially, the excitation is mainly localized on the energy donor and after ∼1 ps, the population slowly starts flowing towards the excited energy acceptor. Energy transfer is accomplished at ∼27.5 ps, where the population is transferred

to the acceptor, as seen by the crossing of the blue and red lines in Fig.4g.

For the RET pair, the dimension of the non adiabatic basis is fairly large: as discussed above, we truncate the dimension of the two Fock spaces associated with the two molecular coordinates as to describe 16 vibrational excitations overall, leading to 544 basis states. Solving the Redfield equation (Eq.9) requires $O(544^3)$ scalar multiplications for each time step, making the calculation very demanding. However, some strategies can be adopted in order to speed the calculations up.[63,65] At time zero, the reduced density matrix is prepared in a coherent state and, as time proceeds, the system relaxes dissipating energy. Accordingly, states lying at energies much higher than the initial coherent state will never be appreciably populated and can be safely neglected. As already observed in Fig.3, the secular approximation and the Bloch model are expected to fail in describing the early-stage dynamics of the coherent state, where population-coherence as well as coherence-coherence transfer phenomena are important. Moreover, the presence of two vibrational modes with similar frequencies in the model in Eq.5 leads to several quasi-degenerate states and to several non-secular $R_{ab,cd}$ components.[68] Consequently, neither the Bloch model nor the secular approximation can be used. In these conditions, the computationally expensive Redfield equation is approximated by a pseudo non-secular algorithm, keeping only those $R_{ab,cd}$ non-secular terms that satisfy the condition $|\omega_{ab} - \omega_{cd}| \leq \alpha$, where α is a fixed threshold.[65]

Fig.5 compares results obtained for the $\mathcal{DA}$ system using the full Redfield equation, the pseudo non-secular algorithm (with α=0.01 eV) and the Bloch model. In the upper panel, the coherent oscillations of the vibrational coordinate of $\mathcal{D}$ obtained within the Bloch model damp faster than those calculated using the full Redfield equation and ruinously diverge after $\sim$200 fs. Indeed, the divergence is fixed accounting for the most important non-secular terms; using the pseudo non-secular algorithm with α=0.01 eV, thus accounting for the 0.006% of the total relaxation super-operator, we obtain results that compare well with those obtained using the full Redfield equation. Moreover, increasing α to 0.2 eV, thus accounting for the 0.12% of the full relaxation tensor, the early-time oscillations of the

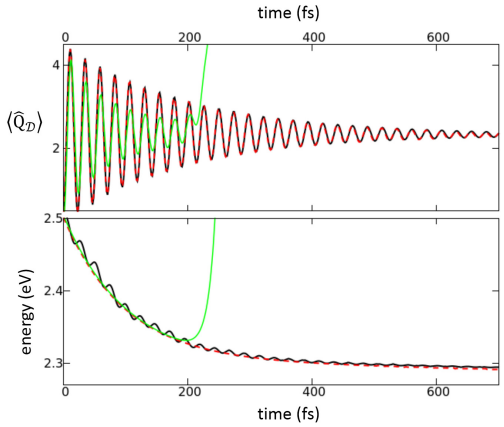

Figure 5: The prominent role of non-secular terms in the multicomponent energy donor-energy acceptor system. Early-stage dynamics of $\langle \hat{Q}_{\mathcal{D}} \rangle$ (upper panel) and of the system energy (lower panel). Continuous black curve: results from full Redfield equation; dashed red curve: results from the pseudo non-secular algorithm with α=0.01 eV; continuous green curve: results from the Bloch model. The same model parameters are used as in Fig.4.

system energy (lower panel) are also prefectly reproduced (results for α=0.2 eV completely overlap full Redfield results and are not shown). Being a good compromise between physical accuracy and computational efficiency, the pseudo non-secular approach with α=0.01 eV was used for the Redfield results shown in this Section.

4.2 Strong coupling regime

The results discussed above for V=0.08 eV match well with the standard Förster picture where $\mathcal{D}^*$ relaxes towards the excited state equilibrium geometry before transferring energy to the acceptor site in an incoherent process. Having a model that explicitly deals with molecular vibrations, we are in the position to look at processes occurring in the strong coupling regime. In the following we discuss results obtained for V=0.3 and 0.6 eV. In Fig.6, Redfield trajectories calculated in the strong coupling limit are shown superimposed to the adiabatic potential energy surfaces. As before, the system is prepared in a coherent state using Eq.6 and only accounting for the $\mathcal{D}$ dipole moment (results for different excitation procedures are shown in the SI). At variance with the weak-coupling case, in the large

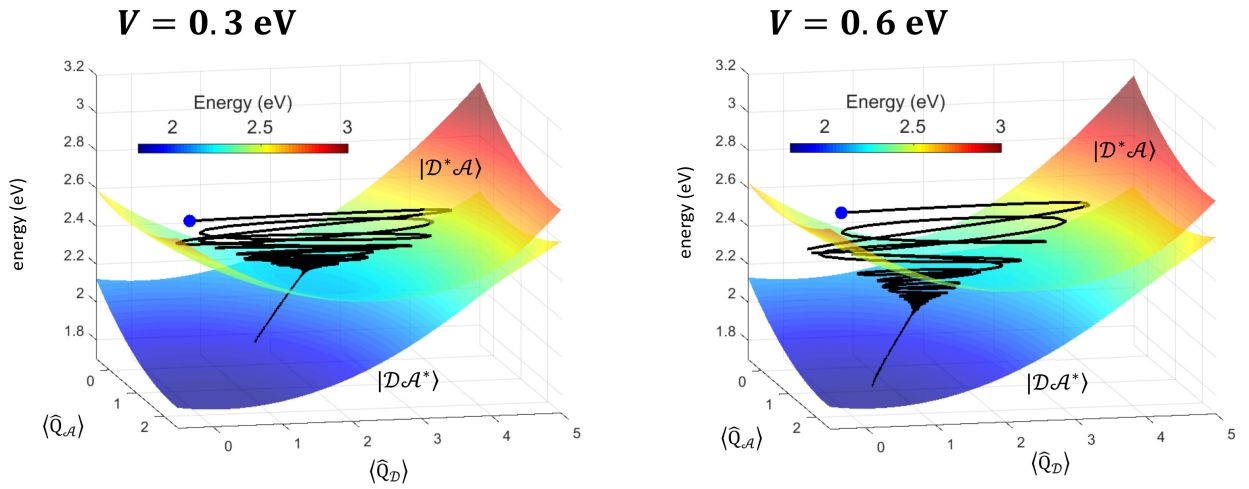

Figure 6: Redfield dynamics calculated for V=0.3 and 0.6 eV (strong coupling regime), using the molecular parameters reported in Tab.1 and setting the non-secular threshold α=0.2 eV. The blue dot marks the starting point of the evolution. The adiabatic potential energy surfaces relevant to $|\mathcal{D}^*\mathcal{A}\rangle$ and $|\mathcal{D}\mathcal{A}^*\rangle$ are shown for reference. The maximum number of vibrational excitations is set to 15 when V=0.3 eV and to 16 when V=0.6 eV. Other parameters are defined in the main text.

coupling case a sizable mixing of the $\mathcal{D}$ and $\mathcal{A}$ states is observed, so that, even if the excitation only directly involves $\mathcal{D}$ states, also the $\mathcal{A}$ molecule is excited, as clearly seen by the $\langle\hat{Q}_\mathcal{A}\rangle$ oscillations that start immediately after photoexcitation (Fig.7d,f) and survive while moving from $|\mathcal{D}^*\mathcal{A}\rangle$ to $|\mathcal{D}\mathcal{A}^*\rangle$ (Fig.6). It is also clear that, particularly for the V=0.6 eV case, the transfer to the $\mathcal{D}\mathcal{A}^*$ surface starts well before the relaxation on the $\mathcal{D}^*\mathcal{A}$ state is completed.

In order to better locate the energy transfer, we plot in the left panels of Fig.7 the population of the two long-living states that are identified as the lowest eigenstate of the relaxed $\mathcal{D}^*\mathcal{A}$ state (roughly corresponding to the lowest vibrational eigenstate associated with the $\mathcal{D}^*\mathcal{A}$ potential energy surface) and the lowest eigenstate of the relaxed $\mathcal{D}\mathcal{A}^*$ state. Immediately after photoexcitation, internal conversion drives the system towards the relaxed $\mathcal{D}^*\mathcal{A}$ state and its population rapidly increases, virtually touching 1 in the weak coupling limit (Fig.7a), before starting to appreciably populate $\mathcal{D}\mathcal{A}^*$ state. By increasing V, the population of the $\mathcal{D}^*\mathcal{A}$ state never attains the 1 value and for V=0.6 eV it barely overcomes

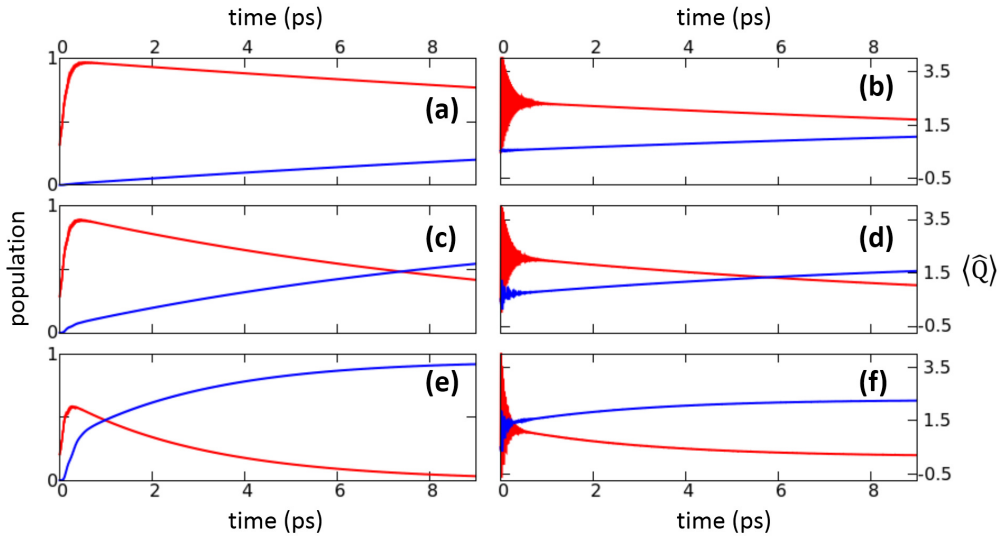

Figure 7: The effect of $\mathcal{DA}$ interaction strength, V, on RET dynamics. Results obtained using pseudo non-secular Redfield equation with threshold α=0.2 eV for V=0.08 (panels a and b), 0.3 (panels c and d), 0.6 eV (panels e and f). Left panels: Time dependence of $\mathcal{D}^*\mathcal{A}$ (red curve) and $\mathcal{DA}^*$ (blue curve) long-living state populations. Right panels: expectation value of $\hat{Q}_{\mathcal{D}}$ (red curve) and $\hat{Q}_{\mathcal{A}}$ (blue curve). All other model parameters are the same as in Fig.4.

0.5. At the same time, the population of the $\mathcal{DA}^*$ state rapidly increases and, identifying the RET time with the point where the red and blue curves cross, we see that RET occurs at ∼27 ps for V=0.08 eV (Fig.4g), ∼7.4 ps for V=0.3 eV, and ∼1 ps for V=0.6 eV.

In order to help the discussion, some auxiliary quantities are defined, namely the purity and the coherence.[65] The purity of a quantum system, $p(t)$=$Tr\{\hat{\sigma}^2(t)\}$, ranges from p=$1/N$ for a fully mixed state to p=1 for a pure state. It is related to the linear entropy of the system by the simple equation $S_l(t) = 1 - p(t)$, so that the entropy increases with decreasing purity. The coherence of the quantum state can be calculated as $C(t) = p(t) - \sum_i \sigma_{ii}^2(t)$. In Fig.8 we report the time-dependence of the purity and of the coherence calculated for the three different V values discussed above. As a result of the dissipative dynamics, the coherence drops down very quickly and is basically negligible after the first 500 fs. Before dying off, the coherence shows distinct oscillations at the vibrational frequency of $\mathcal{D}^*$. Quite interestingly, the stronger entanglement of $\mathcal{D}$ and $\mathcal{A}$ states for large V values makes the

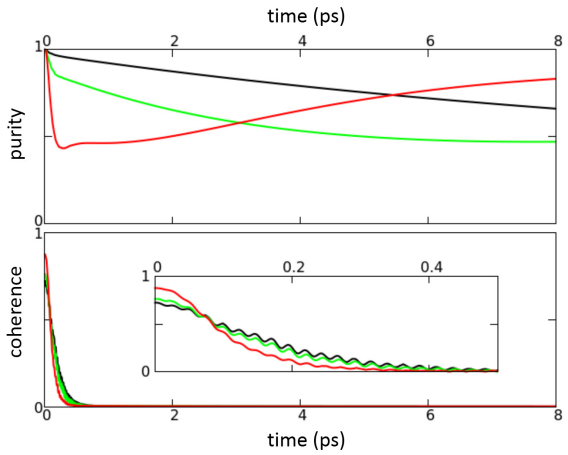

Figure 8: The effect of V on the $\mathcal{SB}$ entanglement and $\mathcal{S}$ decoherence. Time-dependence of purity (upper panel) and coherence (lower panel); the inset is an enlargement of the early-stage time-dependence of coherence. Results are shown for V=0.08 (black curve), 0.3 (green curve), 0.6 eV (red curve). All other parameters are the same as in Fig.7.

decoherence faster. As for purity, the system is prepared in a pure state at time zero (no entropy), and the purity drops down with time as the system explores other states. Actually purity increases again after RET, when the $\mathcal{DA}^*$ starts to be significantly populated.

5 Conclusions

Energy dissipation and relaxation phenomena are central to the physics of photoexcited state dynamics. The interaction of a molecule with the environment is crucial in this respect and brings us into the fascinating field of open quantum systems. In this work, we present a Redfield approach to dissipative non-adiabatic dynamics in single molecules and in a RET pair.

The molecules are described based on a parametric Hamiltonian that reliably describes their low-energy behavior in terms of just two electronic states, coupled to a vibrational coordinate. In the RET pair the two molecules interact via electrostatic interactions. This comparatively simple model makes a truly non-adiabatic approach to the molecular dynamics affordable both for the single molecules and for the RET pair while allowing, at the same

time, to validate approximate approaches to the Redfield dynamics against exact results. The celebrated Bloch model that separates the population and coherence dynamics, works well for a single molecule, but dramatically fails for the RET pair where the presence of two coupled vibrational coordinates with similar frequencies is responsible for the appearance of several quasi-degenerate states. The pseudo non-secular approximation offers a reliable and numerically viable strategy in these conditions.

Despite its comparative simplicity, the proposed model captures the essential physics of the processes of interest. Indeed, for the isolated molecule, the explicit non-adiabatic treatment of molecular vibrations coupled to a Redfield bath, described by the single relaxation parameter γ, rationalizes the basic features of energy dissipation for a molecule interacting with a fast fluctuating environment (homogeneous broadening). In particular two different timescales for relaxation emerge, with a fast (timescales $\sim$100 fs) energy dissipation towards the lowest excited state followed by a much slower relaxation towards the ground state (with typical timescales in the ns regime).

The highly non-trivial results obtained for the isolated molecule set the basis for a dynamical description of RET not only in the weak-coupling regime, where, in line with the Förster model, RET occurs from the relaxed $\mathcal{D}^*$ state, but also in the strong coupling regime where the transfer is effective well before the complete $\mathcal{D}^*$ relaxation. Modeling RET dynamics adds one layer of complexity to the problem, well beyond the computational challenge. The Redfield approach accounts for a single bath, that in RET systems must be coupled to both the energy donor and acceptor molecules (Eq.13). Accordingly, the kinetic coefficients account for exchange energy processes where vibrational quanta are exchanged between the two molecules. In other terms, the coupling of each dye to the common bath introduces a mutual effective coupling between the dyes.[68] This is of course expected for a RET pair where the two molecules are at close distance, so that fluctuations occurring in the close proximity of a molecule are also felt by the other molecule (by the way, since RET is driven by electrostatic forces the two molecules are bound to feel the fluctuation of electric fields).

However this kind of interaction should decrease with the intermolecular distance and virtually vanish for two non-interacting dyes. Formally accounting for this dependence of kinetic coefficients on intermolecular distances would require a more complex bath description, with the bath phonons oscillating both in time and in space in a model that accounts for a wavevector-dependent coupling between the system and the bath. This treatment is well beyond the scope of this paper, but, for the sake of comparison, we did some calculation deleting the mixed $\mathcal{DA}$ terms in Eqs.14 and 15 (see SI). The first important result is obtained for V=0: we do not observe energy transfer neither in the presence nor in the absence of the bath-induced coupling between $\mathcal{D}$-$\mathcal{A}$. For finite V, deleting the mixing terms leads, all other parameters fixed, to a much faster RET, suggesting that the bath-induced $\mathcal{D}$-$\mathcal{A}$ interaction actually slows down the energy transfer opening effective back-transfer channels. On a qualitative perspective, the behavior is similar as in the complete model, and upon increasing V the system is driven from weak to strong coupling. On the other hand, the bath model and its coupling to the system are strictly phenomenological and, in principle, either model can be selected.

Further steps are needed to understand RET in molecular systems, the most challenging and most important being the inclusion of the effects due to polar solvation. Polar solvation enters the essential state models in terms of a reaction field, leading to a reliable description of solvatochromic effects including the highly non-trivial effects of inhomogeneous broadening due to thermal disorder in polar solvents. The same approach is expected to apply to RET, where inhomogeneous broadening and the interplay between the molecular and solvent dynamics can lead to large effects on RET efficiency. Another direction worth to explore concerns RET involving symmetric molecules, to study how dark-states participate to RET in an approach that overcomes the dipolar approximation while maintaining the simplicity of essential state models. In an even more ambitious project, RET involving molecular aggregates must be addressed to study the concurrent dynamics of energy transfer and delocalization. Efforts along these directions are definitely worthwhile and are made viable

by the essential state picture that offers a reliable and flexible strategy to deal with relaxation in molecular systems.

Acknowledgement

This work was supported by Italian MIUR through PRIN 2012T9XHH7 and by CINECA through projects IsC50_MMM-time and IscrC_iiCT-MMM. This research benefits from the HPC (High Performance Computing) facility of the University of Parma, Italy.

Supporting Information Available

See supplementary material for results on the coherently excited isolated Nile Red chromophore. Results obtained for the RET pair using a different excitation model and removing the mixed terms in Eqs.14 and 15 are also reported. This material is available free of charge via the Internet at `http://pubs.acs.org/`.

References

(1) Lakowicz, J. R. *Principles of Fluorescence Spectroscopy*, 3rd ed.; Springer, US, 2006; Chapter 13, p 443.

(2) Valeur, B. *Molecular Fluorescence: Principles and Applications*, 1st ed.; Wiley-VCH Verlag GmbH & Co. KGaA, 2001; Chapter 4, p 110.

(3) Thomas, S. W.; Joly, G. D.; Swager, T. M. Chemical Sensors Based on Amplifying Fluorescent Conjugated Polymers. *Chem. Rev.* **2007**, *107*, 1339–1386.

(4) Swager, T. M. The Molecular Wire Approach to Sensory Signal Amplification. *Acc. Chem. Res.* **1998**, *31*, 201–207.

(5) Currie, M. J.; Mapel, J. K.; Heidel, T. D.; Goffri, S.; Baldo, M. A. High-Efficiency Organic Solar Concentrators for Photovoltaics. *Science* **2008**, *321*, 226–228.

(6) Beljonne, D.; Curutchet, C.; Scholes, G. D.; Silbey, R. J. Beyond Förster Resonance Energy Transfer in Biological and Nanoscale Systems. *J. Phys. Chem. B* **2009**, *113*, 6583–6599.

(7) Scholes, G. D. Long-Range Resonance Energy Transfer In Molecular Systems. *Annu. Rev. Phys. Chem.* **2003**, *54*, 57–87.

(8) Saini, S.; Srinivas, G.; Bagchi, B. Distance and Orientation Dependence of Excitation Energy Transfer: From Molecular Systems to Metal Nanoparticles. *J. Phys. Chem. B* **2009**, *113*, 1817–1832.

(9) Wasielewski, M. R. Photoinduced electron transfer in supramolecular systems for artificial photosynthesis. *Chem. Rev.* **1992**, *92*, 435–461.

(10) Wilson, T.; Hastings, J. W. Bioluminescence. *Annu. Rev. Cell Dev. Biol.* **1998**, *14*, 197–230.

(11) Renger, T. Theory of excitation energy transfer: from structure to function. *Photosynth. Res.* **2009**, *102*, 471–485.

(12) Sundström, V. Femtobiology. *Annu. Rev. Phys. Chem.* **2008**, *59*, 53–77.

(13) Gust, D.; Moore, T. A.; Moore, A. L. Mimicking Photosynthetic Solar Energy Transduction. *Acc. Chem. Res.* **2001**, *34*, 40–48.

(14) Polívka, T.; Frank, H. A. Molecular Factors Controlling Photosynthetic Light Harvesting by Carotenoids. *Acc. Chem. Res.* **2010**, *43*, 1125–1134.

(15) Mirkovic, T.; Ostroumov, E. E.; Anna, J. M.; van Grondelle, R.; Govindjee; Scholes, G. D., Light Absorption and Energy Transfer in the Antenna Complexes of Photosynthetic Organisms. *Chem. Rev.* **2017**, *117*, 249–293.

(16) Renger, T.; May, V.; Kühn, O. Ultrafast excitation energy transfer dynamics in photosynthetic pigment-protein complexes. *Phys. Rep.* **2001**, *343*, 137–254.

(17) Curutchet, C.; Mennucci, B. Quantum Chemical Studies of Light Harvesting. *Chem. Rev.* **2017**, *117*, 294–343.

(18) Förster, T. Zwischenmolekulare Energiewanderung und Fluoreszenz. *Ann. Phys.* **1948**, *437*, 55–75.

(19) Förster, T. 10th Spiers Memorial Lecture. Transfer mechanisms of electronic excitation. *Discuss. Faraday Soc.* **1959**, *27*, 7–17.

(20) Förster, T. Transfer Mechanisms of Electronic Excitation Energy. *Radiat. Res. Supplement* **1960**, *2*, 326–339.

(21) Förster, T. Delocalized excitation and excitation transfer. In *Modern Quantum Chemistry*; Sinaoglu, O., Ed.; Academic Press, New York, 1965; Vol. 111; p 93.

(22) Krueger, B. P.; Scholes, G. D.; Fleming, G. R. Calculation of Couplings and Energy-Transfer Pathways between the Pigments of LH2 by the ab Initio Transition Density Cube Method. *J. Phys. Chem. B* **1998**, *102*, 5378–5386.

(23) Scholes, G. D.; Jordanides, X. J.; Fleming, G. R. Adapting the Förster Theory of Energy Transfer for Modeling Dynamics in Aggregated Molecular Assemblies. *J. Phys. Chem. B* **2001**, *105*, 1640–1651.

(24) Jordanides, X. J.; Scholes, G. D.; Fleming, G. R. The Mechanism of Energy Transfer in the Bacterial Photosynthetic Reaction Center. *J. Phys. Chem. B* **2001**, *105*, 1652–1669.

(25) Madjet, M. E.; Abdurahman, A.; Renger, T. Intermolecular Coulomb Couplings from Ab Initio Electrostatic Potentials: Application to Optical Transitions of Strongly Coupled Pigments in Photosynthetic Antennae and Reaction Centers. *J. Phys. Chem. B* **2006**, *110*, 17268–17281.

(26) Wong, K. F.; Bagchi, B.; Rossky, P. J. Distance and Orientation Dependence of Excitation Transfer Rates in Conjugated Systems: Beyond the Förster Theory. *J. Phys. Chem. A* **2004**, *108*, 5752–5763.

(27) Hsu, C.-P.; Fleming, G. R.; Head-Gordon, M.; Head-Gordon, T. Excitation energy transfer in condensed media. *J. Chem. Phys.* **2001**, *114*, 3065–3072.

(28) Iozzi, M. F.; Mennucci, B.; Tomasi, J.; Cammi, R. Excitation energy transfer (EET) between molecules in condensed matter: A novel application of the polarizable continuum model (PCM). *J. Chem. Phys.* **2004**, *120*, 7029–7040.

(29) Neugebauer, J. Couplings between electronic transitions in a subsystem formulation of time-dependent density functional theory. *J. Chem. Phys.* **2007**, *126*, 134116.

(30) Sissa, C.; Manna, A. K.; Terenziani, F.; Painelli, A.; Pati, S. K. Beyond the Förster formulation for resonance energy transfer: the role of dark states. *Phys. Chem. Chem. Phys.* **2011**, *13*, 12734–12744.

(31) Breuer, H.-P.; Petruccione, F. *The Theory of Open Quantum Systems*; Oxford University Press, 2010; Chapter 3, p 110.

(32) May, V.; Kühn, O. *Charge and Energy Transfer Dynamics in Molecular Systems*, 3rd ed.; Wiley-VCH Verlag GmbH & Co. KGaA, 2011; Chapter 3, p 67.

(33) Ishizaki, A.; Fleming, G. R. On the adequacy of the Redfield equation and related approaches to the study of quantum dynamics in electronic energy transfer. *J. Chem. Phys.* **2009**, *130*, 234110.

(34) Jang, S.; Jung, Y.; Silbey, R. J. Nonequilibrium generalization of Förster-Dexter theory for excitation energy transfer. *Chem. Phys.* **2002**, *275*, 319–332.

(35) Christensson, N.; Kauffmann, H. F.; Pullerits, T.; Mančal, T. Origin of Long-Lived Coherences in Light-Harvesting Complexes. *J. Phys. Chem. B* **2012**, *116*, 7449–7454.

(36) Hughes, K. H.; Christ, C. D.; Burghardt, I. Effective-mode representation of non-Markovian dynamics: A hierarchical approximation of the spectral density. I. Application to single surface dynamics. *J. Chem. Phys.* **2009**, *131*, 024109.

(37) Hwang-Fu, Y.-H.; Chen, W.; Cheng, Y.-C. A coherent modified Redfield theory for excitation energy transfer in molecular aggregates. *Chem. Phys.* **2015**, *447*, 46–53.

(38) Boldrini, B.; Cavalli, E.; Painelli, A.; Terenziani, F. Polar Dyes in Solution: A Joint Experimental and Theoretical Study of Absorption and Emission Band Shapes. *J. Phys. Chem. A* **2002**, *106*, 6286–6294.

(39) Painelli, A. Amplification of NLO responses: vibronic and solvent effects in push-pull polyenes. *Chem. Phys.* **1999**, *245*, 185–197.

(40) Painelli, A.; Terenziani, F. Optical Spectra of Push-Pull Chromophores in Solution: A Simple Model. *J. Phys. Chem. A* **2000**, *104*, 11041–11048.

(41) Terenziani, F.; Painelli, A.; Comoretto, D. Solvation Effects and Inhomogeneous Broadening in Optical Spectra of Phenol Blue. *J. Phys. Chem. A* **2000**, *104*, 11049–11054.

(42) Terenziani, F.; Painelli, A.; Girlando, A.; Metzger, R. M. From Solution to Langmuir-Blodgett Films: Spectroscopic Study of a Zwitterionic Dye. *J. Phys. Chem. B* **2004**, *108*, 10743–10750.

(43) Terenziani, F.; Painelli, A. Supramolecular interactions in clusters of polar and polarizable molecules. *Phys. Rev. B* **2003**, *68*, 165405.

(44) Sanyal, S.; Painelli, A.; Pati, S. K.; Terenziani, F.; Sissa, C. Aggregates of quadrupolar dyes for two-photon absorption: the role of intermolecular interactions. *Phys. Chem. Chem. Phys.* **2016**, *18*, 28198–28208.

(45) Sanyal, S.; Sissa, C.; Terenziani, F.; Pati, S. K.; Painelli, A. Superlinear amplification

of the first hyperpolarizability of linear aggregates of DANS molecules. *Phys. Chem. Chem. Phys.* **2017**, *19*, 24979–24984.

(46) Sissa, C.; Terenziani, F.; Painelli, A.; Manna, A.; Pati, S. Resonance energy transfer between polar charge-transfer dyes: A focus on the limits of the dipolar approximation. *Chem. Phys.* **2012**, *404*, 9–15.

(47) Painelli, A. Vibronic contribution to static NLO properties: exact results for the DA dimer. *Chem. Phys. Lett.* **1998**, *285*, 352–358.

(48) Mulliken, R. S. Molecular Compounds and their Spectra. II. *J. Am. Chem. Soc.* **1952**, *74*, 811–824.

(49) Rice, M. Towards the experimental determination of the fundamental microscopic parameters of organic ion-radical compounds. *Solid State Commun.* **1979**, *31*, 93 – 98.

(50) Painelli, A.; Girlando, A. Electron-molecular vibration (e-mv) coupling in charge-transfer compounds and its consequences on the optical spectra: A theoretical framework. *J. Chem. Phys.* **1986**, *84*, 5655–5671.

(51) Cederbaum, L. S.; Gindensperger, E.; Burghardt, I. Short-Time Dynamics Through Conical Intersections in Macrosystems. *Phys. Rev. Lett.* **2005**, *94*, 113003.

(52) Gindensperger, E.; Burghardt, I.; Cederbaum, . S. Short-time dynamics through conical intersections in macrosystems. I. Theory: Effective-mode formulation. *J. Chem. Phys.* **2006**, *124*, 144103.

(53) Gindensperger, E.; Burghardt, I.; Cederbaum, L. S. Short-time dynamics through conical intersections in macrosystems. II. Applications. *J. Chem. Phys.* **2006**, *124*, 144104.

(54) Picconi, D.; Lami, A.; Santoro, F. Hierarchical transformation of Hamiltonians with linear and quadratic couplings for nonadiabatic quantum dynamics: Application to the $\pi\pi^*/n\pi^*$ internal conversion in thymine. *J. Chem. Phys.* **2012**, *136*, 244104.

(55) Del Freo, L.; Painelli, A. Anharmonicity and NLO responses: an exact diagonalization study. *Chem. Phys. Lett.* **2001**, *338*, 208–216.

(56) Terenziani, F.; Painelli, A. Collective and cooperative phenomena in molecular materials: dimers of polar chromophores. *J. Lumin.* **2005**, *112*, 474–478.

(57) Terenziani, F.; Painelli, A. Two-dimensional electronic-vibrational spectra: modeling correlated electronic and nuclear motion. *Phys. Chem. Chem. Phys.* **2015**, *17*, 13074–13081.

(58) Sissa, C.; Delchiaro, F.; Di Maiolo, F.; Terenziani, F.; Painelli, A. Vibrational coherences in charge-transfer dyes: A non-adiabatic picture. *J. Chem. Phys.* **2014**, *141*, 164317.

(59) Altland, A.; Simons, B. *Condensed Matter Field Theory*, 2nd ed.; Cambridge University Press, UK, 2010; Chapter 11, p 698.

(60) Roden, J.; Strunz, W. T.; Whaley, K. B.; Eisfeld, A. Accounting for intra-molecular vibrational modes in open quantum system description of molecular systems. *J. Chem. Phys.* **2012**, *137*, 204110.

(61) Redfield, A. G. On the Theory of Relaxation Processes. *IBM J. Res. Dev.* **1957**, *1*, 19–31.

(62) Klinduhov, N.; Boukheddaden, K. Vibronic Theory of Ultrafast Intersystem Crossing Dynamics in a Single Spin-Crossover Molecule at Finite Temperature beyond the Born-Oppenheimer Approximation. *J. Phys. Chem. Lett.* **2016**, *7*, 722–727.

(63) Pollard, W. T.; Friesner, R. A. Solution of the Redfield equation for the dissipative quantum dynamics of multilevel systems. *J. Chem. Phys.* **1994**, *100*, 5054–5065.

(64) Am-Shallem, M.; Levy, A.; Schaefer, I.; Kosloff, R. Three approaches for representing Lindblad dynamics by a matrix-vector notation. *ArXiv e-prints* **2015**, arXiv:1510.08634v2 [quant-ph].

(65) Balzer, B.; Stock, G. Modeling of decoherence and dissipation in nonadiabatic photoreactions by an effective-scaling nonsecular Redfield algorithm. *Chem. Phys.* **2005**, *310*, 33–41.

(66) Bloch, F. Nuclear Induction. *Phys. Rev.* **1946**, *70*, 460–474.

(67) Wangsness, R. K.; Bloch, F. The Dynamical Theory of Nuclear Induction. *Phys. Rev.* **1953**, *89*, 728–739.

(68) Eastham, P. R.; Kirton, P.; Cammack, H. M.; Lovett, B. W.; Keeling, J. Bath-induced coherence and the secular approximation. *Phys. Rev. A* **2016**, *94*, 012110.
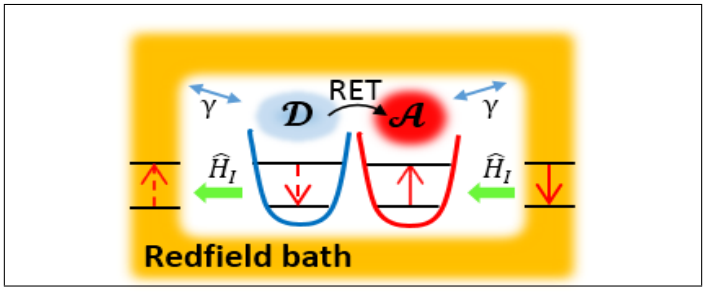
Graphical TOC Entry